minerals

MDPI

Article

Central European Variscan Basement in the Outer Carpathians: A Case Study from the Magura Nappe, Outer Western Carpathians, Poland

Aleksandra Gawęda [1,*], Krzysztof Szopa [1], Jan Golonka [2], David Chew [3] and Anna Waśkowska [2]

[1] Institute of Earth Sciences, University of Silesia in Katowice, Będzińska 60, 41-200 Sosnowiec, Poland; krzysztof.szopa@us.edu.pl
[2] Faculty of Geology, Geophysics and Environmental Protection, AGH University of Science and Technology, al. A. Mickiewicza 30, 30-059 Kraków, Poland; jan_golonka@yahoo.com (J.G.); waskowsk@agh.edu.pl (A.W.)
[3] Department of Geology, School of Natural Sciences, Trinity College Dublin, Dublin 2, Ireland; chewd@tcd.ie
* Correspondence: aleksandra.gaweda@us.edu.pl; Tel.: +48-695091115

Abstract: Exotic crystalline blocks within the Outer Carpathian flysch have the potential to establish the nature of their eroded basement source(s) and thus to reconstruct the paleogeography of the Outer Carpathians. Petrological investigations (including mineral analyses) coupled with zircon and apatite U-Pb dating were performed on an exotic crystalline block within Eocene siliciclastic rocks in the Rača Zone of the Magura Nappe in the Outer Western Carpathians, Poland. This exotic block is a large (c. 1 m diameter) pink porphyritic granitoid block found in the Osielczyk Stream, southeast of Osielec village in the Makowski Beskid mountains. The timing of magmatic crystallization is constrained by a U-Pb zircon age of 315.9 ± 2.6 Ma (MSWD = 0.69), while inherited zircon cores yield Archean (c. 2780 Ma), Cadomian (541.8 ± 6.7 Ma; MSWD = 0.53), Devonian (417 ± 11 Ma; MSWD = 0.57) and Early Variscan (c. 374 Ma) ages. Apatites from the same sample yield a Tera Wasserburg lower intercept U-Pb age of 311.3 ± 7.5 (MSWD = 0.87). The granitoid exhibits geochemical characteristics typical of I-type granites and $\varepsilon Nd_{(316\ Ma)}$ = 2.15 (with a T_{DM} model age of 1.18 Ga) and $^{87}Sr/^{86}Sr_{(316\ Ma)}$ = 0.704710. These data suggest a likely source region in the Saxo-Danubian Granite Belt, which possibly formed the basement of the Fore-Magura Ridge.

Keywords: Carpathians; Magura Nappe; exotic clasts; granitoids; U-Pb dating; zircon; apatite

Citation: Gawęda, A.; Szopa, K.; Golonka, J.; Chew, D.; Waśkowska, A. Central European Variscan Basement in the Outer Carpathians: A Case Study from the Magura Nappe, Outer Western Carpathians, Poland. *Minerals* **2021**, *11*, 256. https://doi.org/10.3390/min11030256

Academic Editor: Manuel Francisco Pereira

Received: 18 January 2021
Accepted: 23 February 2021
Published: 28 February 2021

1. Introduction

The Carpathians mountain chain in Central Europe stretches for more than 1300 km from the eastern Alps and the Vienna Basin to the iron Gate gorge on the river Danube. In the Central Carpathians, Variscan basement massifs are a defining characteristic, while the Outer Carpathians comprise a complex nappe system that formed from the Cretaceous through to Neogene time as a result of the collision of several microplates with the consolidated European Plate [1]. The Pieniny Klippen Belt separates the Central Carpathians from the Outer Carpathians. These nappes are built from sedimentary sequences deposited in the Carpathian basins in the western Tethys Ocean. The Carpathian basins themselves are comprised of two domains: the Silesian domain to the north and the Magura domain to the south, which includes the Magura Basin. The sedimentary sequences of the Magura Basin are now incorporated into the Magura Nappe, which is the largest and southernmost tectonic unit in the Outer Western Carpathians.

Detrital zircon and apatite dating are commonly employed in single-grain detrital provenance studies to yield information on the source area [2,3]. However, single-grain provenance studies often yield ambiguous information due to the presence of recycled components or far-traveled detritus and may not be representative of the region surrounding the depositional basin. Coarse blocks and cobbles in flysch deposits (e.g., transported

by turbidity currents as olistoliths) are a better target for characterizing the locally eroded basement and can provide both petrological and (multiphase) geochronological data. Exotic crystalline clasts are quite common as sand- and pebble-sized clasts in sandstones and conglomerates in the Silesian and Subsilesian nappes of the Outer Carpathians, while large exotic cobbles and blocks, including some of the tens to over 100 m in diameter, which are highly likely proximal to their source [4], are found in the flysch sequences [5–7]. In the Magura Nappe, the exotic blocks are extremely rare and limited mainly to the Krynica Zone, close to the Pieniny Klippen Belt. The Pasierbiec Sandstone Member represents the only horizon in the Magura Nappe where accumulations of larger exotic clasts are found (the Osielec locality in the Rača Zone) and includes several metagabbro-metadiorite exotic cobbles and blocks [7–9]. Based on north-south palaeocurrent directions, the Fore-Magura Ridge is the likely source area [9]. Based on recent field studies, the petrographical variety of exotic clasts at the Osielec locality is greater than was previously supposed. In 2013, 1 m diameter block of pink granite was found within the Eocene strata at Osielec. This paper presents the new petrological and geochronological data on this exotic granitoid exotic block and discusses its affinity and provenance. U-Pb geochronology was undertaken on magmatic zircon and apatite from the clast, and these data are then used to discuss the potential link of the Magura Basin basement with both the Silesian Nappe basement and, on a more regional scale, the Central European Variscan Belt.

2. Geological Setting and Sampling

The Outer Western Carpathians (Figure 1a–c) are comprised of a stack of nappes and thrust-sheets containing up to 6 km of Upper Jurassic–Miocene continuous flysch sequences, which were thrust over the European Platform and the autochthonous Miocene cover of the Carpathian Foredeep during Alpine orogenesis. The nappe sequences in the Outer Western Carpathians were detached from their basement [10,11] and are comprised of the Magura Nappe, the Fore-Magura Group of Nappes, the Silesian Nappe, the Subsilesian Nappe and the Skole (Skiba) Nappe (Figure 1c). In Poland, the Magura Nappe is composed of Jurassic to Neogene deposits, up to a few thousand meters thick (e.g., [12–14]). It is divided into the Krynica, Bystrica, Rača and Siary subunits (Figure 1d; e.g., [14,15] and references therein).

Two samples, weighing c. 5 kg each from a poorly rounded pink granitoid block (100 cm × 60 cm × 35 cm in size; Figure 2a), were collected from the Rača Zone of the Magura Nappe (Figure 1b). It was found in Osielczyk Stream, in the southeastern part of Osielec village in the Makowski Beskid mountains (grid reference: 49°40′55.9″ N, 19°46′13.6″ E). The boulder lies within the Middle Eocene Pasierbiec Sandstone Member of the Beloveža Formation [16]. The outcrop is located within the Northern Osielczyk thrust sheet of the Osielec Skiba (duplex) [9] (Figure 1b). The Pasierbiec Sandstone Member in the Rača Zone is comprised of fine- to coarse-grained sandstones, conglomeratic sandstones and coarse conglomerates, which are predominantly thickly bedded with subordinate intercalations of muddy shales (Figure 1c). In the sandstones and conglomerates, clasts of schist, granitoid, gneiss, amphibolite and sedimentary rock occur [17]. It is important to note that the occurrence of granitoid clasts larger than a few cm is unique both in the Osielczyk Stream locality and in the Magura Nappe as a whole. Near the granitoid boulder locality, chaotic olistostrome deposits occur. Several metadiorite–metagabbro cobles and blocks have been described from this olistostrome [7,8].

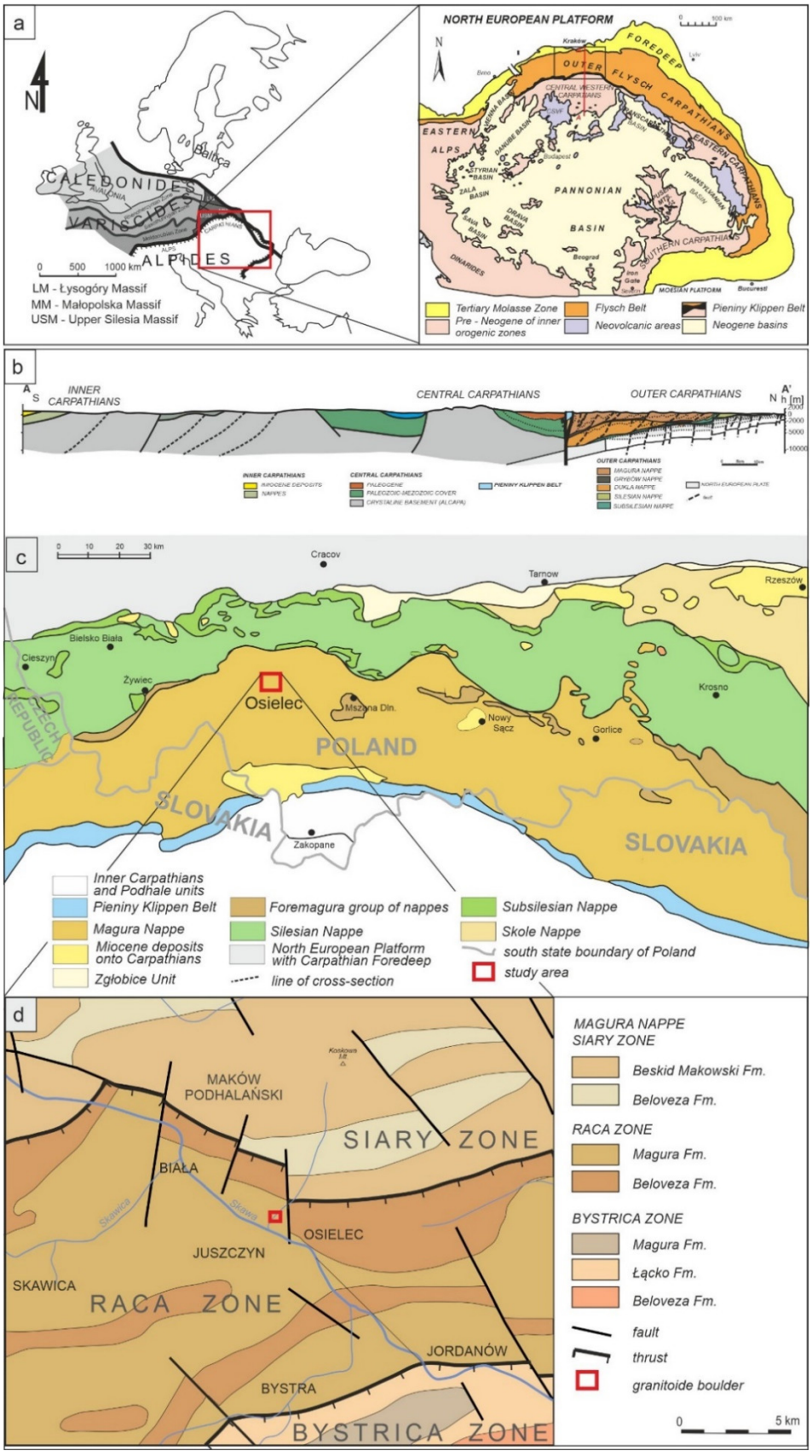

Figure 1. (**a**) A simplified geological sketch of the Carpathian chain within Europe; (**b**) generalized cross-section through the Western Carpathians (modified from [1]); (**c**) the simplified geological map of the Outer Western Carpathians and (**d**) the study area with the locations of the sampling point.

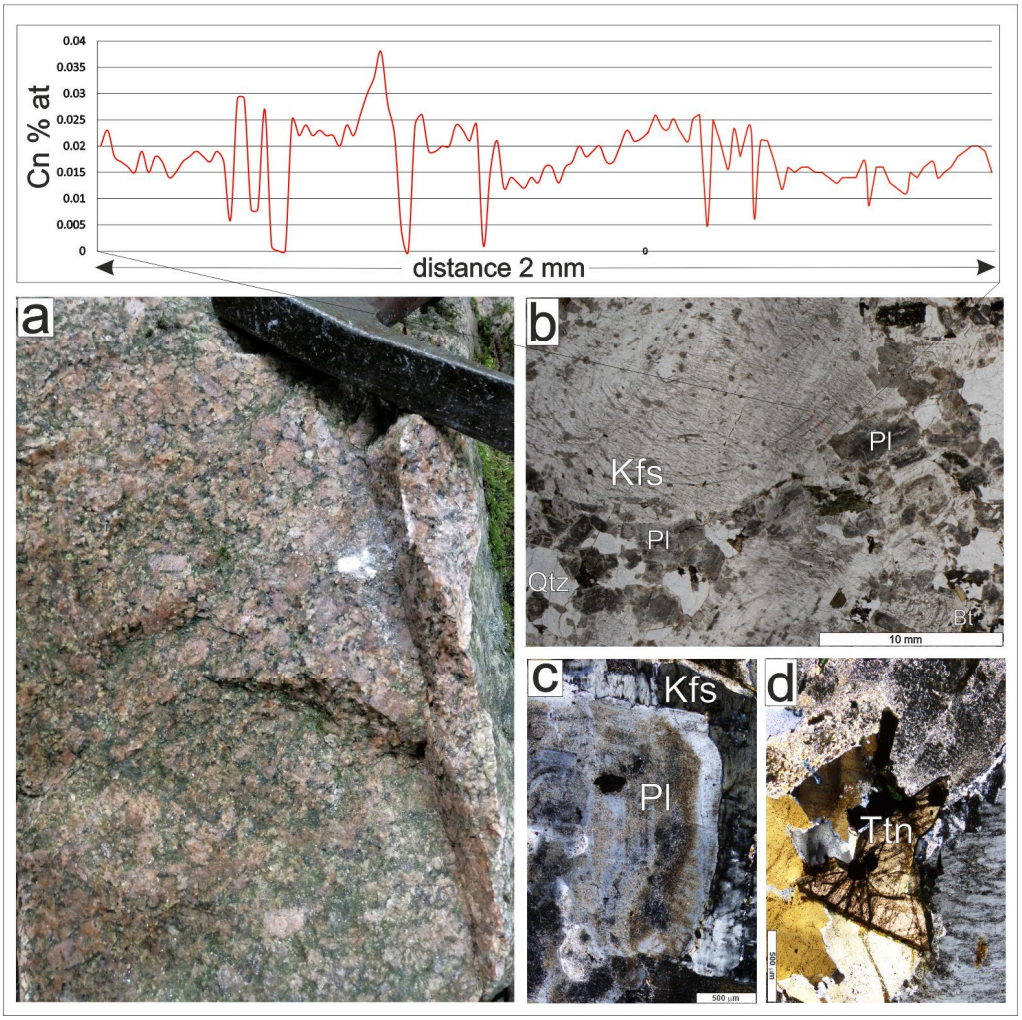

Figure 2. Petrographical features of the granitoid exotic block in different scales: (**a**) field image showing the porphyrocrystals of pink K-feldspars; (**b**) microphotograph showing the zonation of K-feldspar (Kfs) with the barium content profile (as celsjan molecule atomic percent) and its perthitic character (plane-polarized light); (**c**) zoned plagioclase (Pl) crystal, partially sericitized (crossed polarizers); (**d**) titanite crystal (Ttn) crystallizing as a late phase in the space between the feldspars.

3. Analytical Techniques

3.1. Microscopy

Petrographic analyses of thin sections were undertaken at the Institute of Earth Sciences in the University of Silesia in Katowice using an Olympus BX-51 microscope to constrain textural and microstructural relationships and to determine the presence of zircon. The petrographical observations were used to select representative samples for subsequent electron probe microanalysis and whole-rock geochemical analyses.

3.2. Electron Probe Microanalyses (EPMA)

Microprobe analyses of the main rock-forming and accessory minerals were carried out at the Inter-Institutional Laboratory of Microanalyses of Minerals and Synthetic Substances, Warsaw, using a CAMECA SX-100 electron microprobe. The analytical conditions employed an accelerating voltage of 15 kV, a beam current of 20 nA, counting times of 4 s for peak and background and a beam diameter of 1–5 µm. Reference materials, analytical lines, diffracting crystals, mean detection limits (in wt %) and uncertainties were as follows: rutile—Ti (Kα, PET, 0.03, 0.05), diopside—Mg (Kα, TAP, 0.02, 0.11), Si—(Kα, TAP, 0.02, 0.21), Ca—(Kα, PET, 0.03, 0.16), orthoclase—Al (Kα, TAP, 0.02, 0.08), and K (Kα, PET, 0.03,

0.02), albite—Na (Kα, TAP, 0.01, 0.08), hematite—Fe (Kα, LIF, 0.09, 0.47), rhodonite—Mn (Kα, LIF, 0.03, 0.10), phlogopite—F (Kα, TAP, 0.04, 0.32), tugtupite—Cl (Kα, PET, 0.02, 0.04), Cr_2O_3—Cr (Kα, PET, 0.04, 0.01), ZirconED2—Zr (Lα, PET, 0.01, 0.01), Nb_2O_3-MAC—Nb (Lα, PET, 0.09, 0.01), V_2O_5—V (Kα, LIF, 0.02, 0.01), YPO_4—Y (Lα, TAP, 0.05, 0.05), CeP_5O_{14}—Ce (Lα, LPET, 0.09, 0.02), $NdGaO_3$—Nd (Lβ, LIF, 0.31, 0.24), ThO_2—Th (Mα, LPET, 0.09, 0.09), UO_2—U (Mα, LPET, 0.16, 0.13).

3.3. Whole-Rock Chemical and Isotope Analyses

Whole-rock analyses were undertaken by X-ray fluorescence (XRF) for major and large ion lithophile trace elements (LILE) and by fusion and ICP-MS for high field strength elements (HFSE) and rare earth elements (REE) at Bureau Veritas Minerals (Canada). Preparation involved lithium borate fusion and diluted digestions for XRF and lithium borate decomposition or aqua regia digestion for ICP-MS. Loss on ignition (LOI) was determined at 1000 °C. Uncertainties for most of the major elements are 0.01%, except for SiO_2, which is 0.1%. REE was normalized to C1 chondrite [18].

The Sm-Nd and Rb-Sr analytical work was performed at the Laboratory of Geochronology, Department of Lithospheric Research, University of Vienna. Results are based on IC-TIMS procedures. Sample digestion for Nd-Sr analysis was performed in Savillex® beakers using an ultrapure 4:1 mixture of HF and HNO_3 for 10 days at 110 °C on a hot plate. For whole-rock powders, a minimum dissolution time of three weeks was applied to ensure maximum leaching of the REEs from a refractory material, such as zircon. After evaporating the acids, repeated treatment of the residue using HNO_3 and 6.0 N HCl resulted in clear solutions for all samples. The REE fraction was extracted using AG® 50 W-X8 (200–400 mesh, Bio-Rad) resin and 4.0 N HCl. Nd was separated from the REE fraction using Teflon-coated HdEHP and 0.22 N HCl as the elution media. For Sr, element separation followed conventional techniques, using AG® 50W-X8 (200–400 mesh, Bio-Rad) resin and 2.5 N HCl as eluants. Maximum total procedural blanks were <1 ng for Sr and 50 pg for Nd and were taken as negligible. Nd and Sr were run as metals on a Re double filament, using a ThermoFinnigan® Triton MC TIMS. A $^{143}Nd/^{144}Nd$ ratio of 0.511841 ± 0.000005 (n = 5) and an $^{87}Sr/^{86}Sr$ ratio of 0.710259 ± 0.000005 (n = 5) was determined for the La Jolla (Nd) and the NBS987 (Sr) international standards, respectively, during the period of investigation. Within-run mass fractionation for Nd and Sr isotope compositions (IC) was corrected to $^{146}Nd/^{144}Nd = 0.7219$ and $^{86}Sr/^{88}Sr = 0.1194$, respectively. Uncertainties on the Nd and Sr isotope ratios are quoted typically as $2\sigma_m$.

3.4. Mineral Separation and Imaging

Zircon and apatite crystals were separated using standard density separation techniques (crushing, sieving, washing and panning). This separation was carried out at the Institute of Geological Sciences at the Polish Academy of Sciences, Kraków, Poland. The zircons were hand-picked under a binocular microscope, cast in 25 mm diameter epoxy resin mounts, and then ground and polished to expose the grain interiors. Mineral textures were then imaged using back-scattered electron (BSE) and cathodoluminescence (CL) detectors on a FET Philips 30 scanning electron microscope with a 15 kV accelerating voltage and a beam current of 1 nA at the Faculty of Natural Sciences, the University of Silesia in Katowice, Poland.

3.5. LA-ICP-MS U-Pb Dating

3.5.1. Zircon U-Pb Dating

LA-ICPMS U-Pb age data were acquired using a Photon Machines Analyte Excite 193 nm ArF excimer laser-ablation system with a HelEx 2-volume ablation cell coupled to an Agilent 7900 ICPMS at the Department of Geology, Trinity College Dublin. The instruments were tuned using NIST612 standard glass to yield Th/U ratios of unity and low oxide production rates (ThO^+/Th^+ typically <0.15%). A repetition rate of 11 Hz and a circular spot of 24 μm were employed. A quantity of 0.4 $L \cdot min^{-1}$ He carrier gas was fed into the

laser cell, and the aerosol was subsequently mixed with 0.6 L·min^{-1} Ar make-up gas and 11 mL·min^{-1} N_2. Eleven isotopes (^{49}Ti, ^{91}Zr, ^{175}Lu, ^{202}Hg, ^{204}Pb, ^{206}Pb, ^{207}Pb, ^{208}Pb, ^{232}Th, ^{23}5U and ^{23}8U) were acquired during each analysis, which comprised 27 s of ablation and 12 s washout, the latter portions, of which were used for the baseline measurement. Data reduction of the raw U-Pb isotope data was performed through the "VizualAge" data reduction scheme [19] in the freeware IOLITE package [20]. Sample-standard bracketing was applied after the correction of downhole fractionation to account for long-term drift in isotopic or elemental ratios by normalizing all ratios to those of the U-Pb reference standards. Final age calculations were made using the Isoplot add-in for Excel [21]. 91500 zircon (^{206}Pb/^{238}U TIMS age of 1065.4 ± 0.6 Ma; [22]) was used as the primary U-Pb calibration standard. The secondary standards GZ-7 zircon (^{206}Pb/^{238}U TIMS age of 530.26 Ma ± 0.05 Ma; [23]), Plešovice zircon (^{206}Pb/^{238}U TIMS age of 337.13 ± 0.37 Ma; [24]) and WRS 1348 zircon (^{206}Pb/^{238}U TIMS age of 526.26 ± 0.70; [25]) yielded LA-ICPMS ages of 532.0 ± 2.2 Ma, 337 ± 1.6 Ma and 528.4 ± 3.2 Ma, respectively.

3.5.2. Apatite U-Pb Dating

Apatite crystals were as separates on polished epoxy mounts. U-Pb and REE data were acquired using a laser ablation system (Photon Machines Analyte Excite 193 nm ArF Excimer) coupled to an Agilent 7900 Q-ICPMS at the Department of Geology, Trinity College Dublin. Twenty-nine isotopes (^{31}P, ^{35}Cl, ^{43}Ca, ^{51} V, ^{55}Mn, ^{88}Sr, ^{89}Y, ^{90}Zr, ^{139}La, ^{140}Ce, ^{141}Pr, ^{146}Nd, ^{147}Sm, ^{153}Eu, ^{157}Gd, ^{159}Tb, ^{163}Dy, ^{165}Ho, ^{166}Er, ^{169}Tm, ^{172}Yb, ^{175}Lu, ^{202}Hg, ^{204}Pb, ^{206}Pb, ^{207}Pb, ^{208}Pb, ^{232}Th and ^{238}U were acquired using a 60 µm laser spot, a 11 Hz laser repetition rate and a fluence of 2.5 J/cm^2. A ~1 cm sized crystal of Madagascar apatite, which has yielded a weighted average ID-TIMS concordia age of 473.5 ± 0.7 Ma, was used as the primary apatite reference material in this study. McClure Mountain syenite apatite (the rock from which the ^{40}Ar/^{39}Ar hornblende standard MMhb is derived) and Durango apatite were used as secondary standards. McClure Mountain syenite has moderate but reasonably consistent U and Th contents (~23 ppm and 71 ppm, [26]) and its thermal history, crystallization age (weighted mean ^{207}Pb/^{23}5U age of 523.51 ± 2.09 Ma) and initial Pb isotopic composition (^{206}Pb/^{204}Pb = 17.54 ± 0.24; ^{207}Pb/^{204}Pb = 15.47 ± 0.04) are known from high-precision ID-TIMS analyses [27]. NIST 612 standard glass was used as the apatite trace-element reference material, and a crushed aliquot of Durango apatite that has been characterized by solution quadrupole-ICP-MS analyses [28] was used as the apatite trace-element secondary standard.

The raw isotope data were reduced using a modified version of the "Vizual Age" data reduction scheme [19] of the freeware IOLITE package of [25]. This data-reduction scheme ("VizualAge_UcomPbine") can account for the variable common Pb in the apatite [29]. User-defined time intervals are established for the baseline correction procedure to calculate session-wide baseline-corrected values for each isotope. The time-resolved fractionation response of individual standard analyses is then characterized using a user-specified down-hole correction model (such as an exponential curve, a linear fit or a smoothed cubic spline). The data-reduction scheme then fits this appropriate session-wide "model" U-Th-Pb fractionation curve to the time-resolved standard data and the unknowns. Sample-standard bracketing is applied after the correction of down-hole fractionation to account for long-term drift in isotopic or elemental ratios by normalizing all ratios to those of the U-Pb reference standards. Common Pb in the apatite standards and unknowns was corrected using a ^{207}Pb-based correction in VizualAge_UcomPbine and included the propagation of the uncertainties in the age of the reference materials. Over the course of analyses, McClure Mountain apatite (^{207}Pb/^{235}U TIMS age of 523.51 ± 2.09 Ma; [27]) and Durango apatite (31.44 ± 0.18 Ma; [30]) yielded weighted average ^{207}Pb-corrected ages of 517.5 ± 3.5 Ma (MSWD = 2.3) and 31.82 ± 0.41 Ma (MSWD = 1.9), respectively. The McClure Mountain apatite age was anchored using a ^{207}Pb/^{206}Pb value of 0.88198 derived from an apatite ID-TIMS total U-Pb isochron [27]. All apatite REE contents were normalized to C1 chondrite [18].

4. Results

4.1. Petrography, Mineral Chemistry and Whole-Rock Chemistry of Granitoid Exotic Block

Two samples of pink porphyritic granitoid (OS-1 and OS-2; Figure 2a) were collected from one block. The rock is composed of perthitic K-feldspar phenocrysts up to 5 cm long, which usually show twinning (Figure 2b). The barium content ranges from 0.56 to 2.06 wt % and shows oscillatory zonation, with a general decrease in Ba contents towards the rim (Figure 2b). Locally anti-rapakivi structures are observed, characterized by K-feldspar overgrowths on plagioclase. The plagioclase is oligoclase ($An_{11–17}$). Biotite exhibiting green pleochroism is enriched in Mg (#mg = 0.54–0.57; Table 1) and weakly chloritized. No muscovite was noted, but amphibole (Mg-hornblende; Table 2) intergrown with REE-bearing titanite (Table 3) is present. Accessory phases are represented by chemically zoned pyrite, mostly replaced by secondary hydroxides (Ca,F)-apatite enriched in REE and zoned in respect of these elements (Table S1) and zircon. Secondary epidote (Table 3) and hematite are also found.

Table 1. Representative electron microprobe analyses (EMPA) of biotite crystal and their chemical formulae calculated on the basis of 22 O^{2-}.

Compound	LoD	Bt-1	Bt-2	Bt-3	Bt-4
SiO_2 (wt %)	0.04	38.20	38.53	38.32	38.52
TiO_2	0.06	2.54	3.06	2.88	2.88
Al_2O_3	0.03	13.85	13.60	13.75	13.90
Cr_2O_3	0.01	0.05	0.05	b.d.l.	b.d.l.
FeO	0.08	17.75	17.86	17.87	17.70
MgO	0.02	12.49	12.64	1.58	12.57
MnO	0.02	0.74	0.56	0.58	0.74
Na_2O	0.04	0.06	0.06	0.04	0.07
K_2O	0.05	9.69	9.73	9.43	9.35
BaO	0.01	0.16	0.18	0.12	0.25
Total		95.52	96.28	95.58	96.09
Si (a.p.f.u.)		5.791	5.792	5.791	5.792
Al^{iv}		2.208	2.208	2.209	2.208
Al^{vi}		0.265	0.201	0.241	0.255
Ti		0.289	0.346	0.328	0.326
Cr		0.006	0.006	-	-
Fe		2.251	2.246	2.259	2.226
Mg		2.823	2.834	2.833	2.819
Mn		0.095	0.071	0.075	0.107
Na		0.018	0.017	0.013	0.021
K		1.874	1.865	1.819	1.793
Ba		0.009	0.011	0.007	0.015
#mg		0.546	0.550	0.548	0.547

Note: b.d.l.—below detection limit, #mg = Mg/(Fe + Mg + Mn).

Table 2. Chemical composition and crystal-chemical formulae of amphiboles from the exotic mafic blocks from Osielec village (Magura Nappe).

Compound	LoD	#1	#2	#3	#4
SiO_2 (wt %)	0.02	48.99	48.73	48.55	47.1
TiO_2	0.03	0.48	0.52	0.76	1.02
Cr_2O_3	0.01	0.01	0.02	**b.d.l.**	**b.d.l.**
Al_2O_3	0.01	5.37	5.56	5.51	6.23
FeO	0.07	15.21	15.59	14.94	16
MnO	0.06	1.04	1.19	1.23	1.23
MgO	0.02	13.04	12.87	13.00	12.1
CaO	0.02	11.33	11.46	11.46	11.4

Table 2. *Cont.*

Compound	LoD	#1	#2	#3	#4
Na_2O	0.02	1.32	1.38	1.27	1.41
K_2O	0.01	0.54	0.60	0.57	0.66
Total		**96.98**	**96.10**	**96.74**	**97.25**
Fe_2O_3		5,24	5.31	4.94	5.07
FeO*		10.5	10.81	10.49	11.42
H_2O		2.04	2.04	1.99	2.01
Crystal-chemical formulae based on 13-CNK					
Si (a.p.f.u.)		7.178	7.124	7.129	6.987
Al^{IV}		0.822	0.876	0.871	1.013
M1. M2 and M3 sites					
Al^{VI}		0.105	0.082	0.083	0.076
Ti		0.053	0.057	0.084	0.114
Cr		0.001	0.002	0.000	0.000
Fe^{3+}		0.577	0.584	0.546	0.565
Fe^{2+}		1.286	1.322	1.289	1.417
Mn		0.129	0.147	0.153	0.155
Mg		2.848	2.805	2.846	2.674
M4 site					
Ca		1.779	1.795	1.803	1.807
Na		0.221	0.205	0.197	0.193
A site					
Na		0.154	0.186	0.165	0.213
K		0.101	0.112	0.107	0.125
OH		1.998	1.986	1.951	1.990
#mg		0.689	0.680	0.688	0.654
T (°C)		745	754	757	779

Note: b.d.l.—below detection limit, #mg = Mg/(Fe+Mg+Mn).

Table 3. Representative electron microprobe analyses (EMPA) of epidote and titanite crystal and their chemical formulae calculated on the basis of 25 O^{2-} and 5 O^{2-}, respectively.

Compound	LoD	Epidote		Titanite	
		Ep#1	Ep#2	Ttn#1	Ttn#2
V_2O_5 (wt %)	0.1	-	-	0.16	0.16
Nb_2O_5	0.05	-	-	0.87	0.48
SiO_2	0.05	37.71	37.71	29.85	30.51
TiO_2	0.03	0.03	0.11	35.66	36.37
ThO_2	0.05	-	-	0.09	**b.d.l.**
Al_2O_3	0.01	22.56	24.09	1.19	1.41
La_2O_3	0.1	-	-	0.24	**b.d.l.**
Ce_2O_3	0.05	-	-	1.09	0.32
Nd_2O_3	0.19	-	-	0.55	**b.d.l.**
Y_2O_3	0.1	-	-	0.27	**b.d.l.**
Fe_2O_3	0.07	14.1	12.06	2.21	1.69
CaO	0.03	23.07	23.84	26.84	28.53
MnO	0.05	0.32	0.17	0.13	0.19
H_2O_{calc}	-	1.87	1.84	-	-
F	0.03	-	-	0.45	0.95
O=F		-	-	0.25	0.49

Table 3. *Cont.*

Compound	LoD	Epidote		Titanite	
		Ep#1	**Ep#2**	**Ttn#1**	**Ttn#2**
Total		99.66	99.82	99.6	100.61
Nb^{5+} (a.p.f.u.)				0.01	0.01
Si^{4+}		6.03	6.06	1.00	0.99
Ti^{4+}		0.00	0.00	0.89	0.89
Al^{3+}		4.25	4.09	0.05	0.05
Ce^{3+}				0.01	
Fe^{3+}		1.70	1.93	0.06	0.04
Ca^{2+}		3.95	3.81	0.96	0.99
Mn^{2+}		0.04	0.05		0.01
F				0.05	0.10
$\sum_{cations}$		**15.98**	**15.93**	**2.98**	**2.97**

Note: b.d.l.—below detection limit.

The granitoid from Osielec is weakly peraluminous, with Aluminium Saturation Index (ASI) at 1.05 and 1.08; (Table 4) and plot in the Q-monzonite transitional to granite field and belong to the high- K calc-alkaline series (Figure 3a,b). It is enriched in REE ($\sum_{REE}$ = 248 and 351.69; Table 4) and REE patterns are steeply inclined (Ce_N/Yb_N = 24.81 and 36.38) with a very flat Eu anomaly (Eu/Eu* = 0.92 and 0.83; Table 5; Figure 3c). The Rb/Sr ratio is moderate (0.1 and 0.12), and thorium is strongly enriched over uranium (Th/U = 12.7 and 23.6). Zircon saturation temperatures calculated on the basis of the whole-rock Zr content [31] yield temperatures of 814 °C and 853 °C (Table 4), while amphibole thermometry [32] yields a temperature range of 745–780 °C at pressures from 730 to 920 MPa and a $\log \int O_2$ of c. −13 (Table 2).

Table 4. Chemical composition and selected petrological indices of the whole-rock samples of exotic crystalline blocks.

Compound	LoD	Os 1a	Os 1b
SiO_2 (wt %)	0.01	68.96	69.2
TiO_2	0.01	0.33	0.24
Al_2O_3	0.01	15.30	15.8
Fe_2O_3T	0.04	2.98	2.27
MnO	0.01	0.05	0.05
MgO	0.01	0.78	0.62
CaO	0.01	1.43	1.63
Na_2O	0.01	4.62	4.85
K_2O	0.01	4.17	4.09
P_2O_5	0.01	0.21	0.11
LOI	-	0.91	1.12
Total		**99.74**	**99.98**
Sr (ppm)	0.5	1116.00	1271.3
Ba	1.0	1758.00	1650
Rb	0.1	139.80	130.9
Th	0.2	59.10	30.4
U	0.1	2.50	2.4
Ga	0.5	20.30	20.3
Ni	0.1	8.10	6.6
Cr	5.0	42.00	40
Zr	0.1	309.70	207.9
Hf	0.1	8.10	5.5
Y	0.1	14.00	12.3

Table 4. *Cont.*

Compound	LoD	Os 1a	Os 1b
Nb	0.1	35.90	26.2
Ta	0.1	2.10	1.9
La	0.1	96.20	68.3
Ce	0.1	167.60	114.3
Pr	0.02	15.77	11.26
Nd	0.30	52.00	37.3
Sm	0.05	7.22	5.54
Eu	0.02	1.53	1.38
Gd	0.05	4.41	3.76
Tb	0.01	0.50	0.48
Dy	0.05	3.06	2.42
Ho	0.02	0.44	0.44
Er	0.03	1.36	1.22
Tm	0.01	0.19	0.19
Yb	0.05	1.21	1.21
Lu	0.01	0.20	0.2
ASI		1.077	1.046
Rb/Sr		0.125	0.103
Nd/Th		0.88	1.23
Σ_{REE}		351.69	248.00
Eu/Eu*		0.83	0.92
CeN/YbN		36.38	24.81
T_{Zr} (°C)		854	814

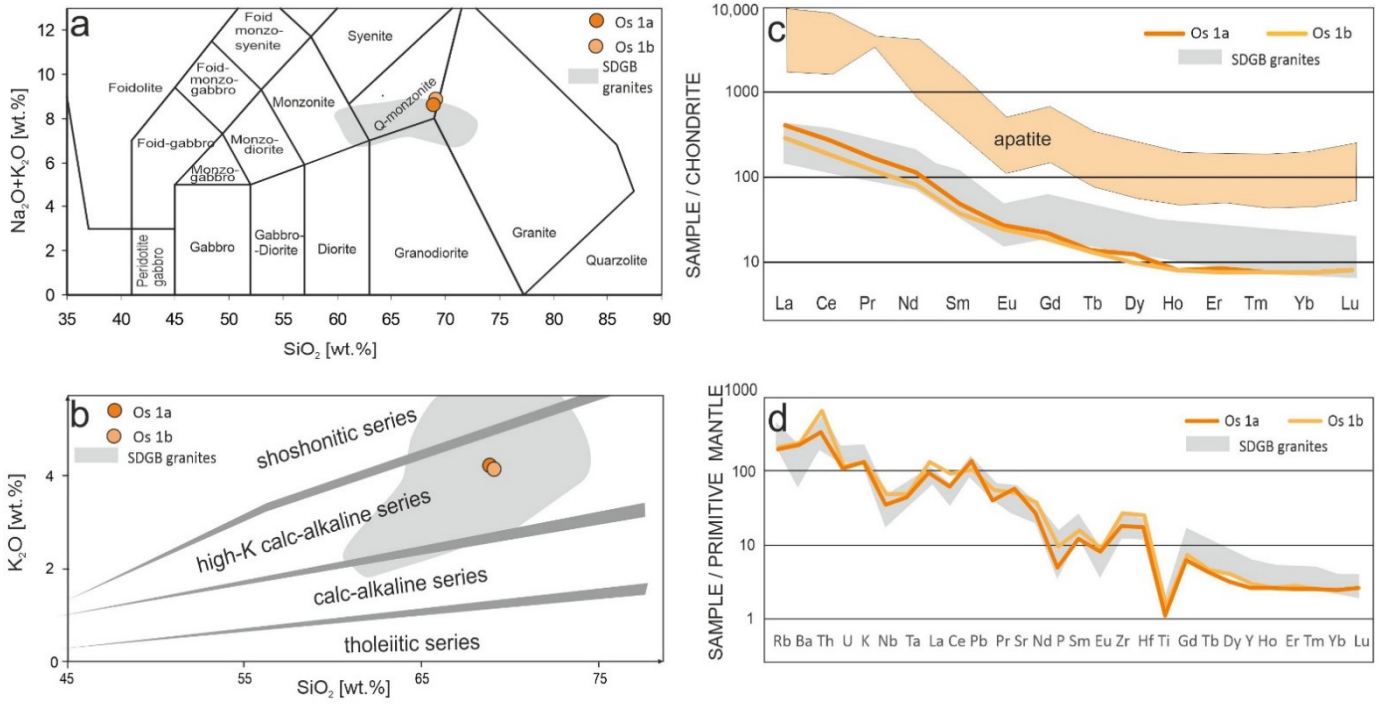

Figure 3. Classification position of the granitoid from Osielec in (**a**) alkali (K_2O + Na_2O) versus SiO_2 TAS classification diagram after [33]; (**b**) K_2O versus SiO_2 classification diagram after [34]; (**c**) chondrite (C1)-normalized REE patterns of the granitoid from Osielec and apatite from the sample (gray area); (**d**) primitive mantle normalized multielement patterns of the analyzed exotic block from Osielec stream. Normalization values after [18], gray field—analyses from [35].

Table 5. U-Pb zircon data from the exotic crystalline block from Osielec.

Sample	Pb^{207}/U^{235}	2s	Pb^{206}/U^{238}	2s	Rho	$^{207}Pb/^{23}5U$ Age (Ma)	2s	$^{206}Pb/^{238}U$ Age (Ma)	2s	U (ppm)	Th (ppm)	Th/U
OS1-1	0.363	0.0065	0.0495	0.00072	0.27601	314.3	4.9	311	4.4	1488	396	0.27
OS1-6	0.372	0.012	0.0506	0.0009	0.22542	320.5	9	318.1	5.5	425.7	59.4	0.14
OS1-7	0.3597	0.0097	0.05	0.00091	0.023636	311.6	7.2	314.5	5.6	581	59.4	0.1
OS1-8	0.374	0.012	0.05122	0.00097	0.17951	321.8	8.9	321.9	5.9	439	464	1.06
OS1-10	0.3669	0.0074	0.04928	0.00071	0.35341	317.1	5.5	310.1	4.3	1944	1168	0.6
OS1-11	0.361	0.011	0.04988	0.00085	0.29725	312.6	8.5	313.7	5.2	492	339	0.69
OS1-15	0.3597	0.0098	0.05006	0.00077	0.055372	311.8	7.2	314.9	4.7	1290	627	0.49
OS1-17	0.369	0.18	0.0509	0.0041	0.55888	318.6	80	319.8	25	1434	677	0.47
OS1-18	0.3728	0.0095	0.05164	0.00097	0.3468	321.4	7	324.6	5.9	1542	790	0.51
OS1-20	0.3684	0.011	0.0516	0.0012	0.4033	318.2	7.9	324.1	7.1	1100	1258	1.14
Concordia age = 315.9 ± 2.5 Ma (MSWD = 0.41)												
INHERITED CORES												
OS1-3	0.447	0.013	0.06051	0.00098	0.038413	374.8	9.3	378.7	6	407	374	0.92
OS1-9	0.528	0.018	0.0688	0.0014	0.25231	430	12	429	8.5	219	36.6	0.17
OS1-16	0.493	0.019	0.0661	0.0016	0.5769	406	13	412.2	9.7	266	90.5	0.34
OS1-21	0.502	0.015	0.0655	0.0012	0.66852	414.1	9.1	408.9	7.1	559	116	0.21
Concordia age = 417.0 ± 11 Ma (MSWD = 0.57)												
OS1-5	0.737	0.028	0.089	0.0023	0.4943	561	16	549	13	154.5	44.5	0.29
OS1-25	0.707	0.029	0.0874	0.0027	0.60153	541	17	540	16	230	244	1.06
OS1-24	0.684	0.029	0.0871	0.0018	0.0628	527	17	538	9.3	104.1	38	0.37
Concordia age = 541.8 Ma (MSWD = 0.53)												
OS1-23	0.85	0.045	0.1025	0.0021	0.15261	619	25	629	11	77.7	72.1	0.93
OS1-19	14.5	0.36	0.538	0.011	0.8371	2780	26	2772	46	99.1	60.1	0.61

4.2. LA-ICP MS U-Pb Dating

4.2.1. Zircon Morphology and U-Pb Dating

Zircon crystals from sample OS-1 are clear, colorless or yellow to gray, with aspect ratios ranging from 1.5:1 to 3:1 and long axes ranging from 50 to 180 µm. Cathodoluminescence (CL) imaging reveals the presence of magmatic oscillatory zoning, locally overgrowing inherited cores showing bright luminescence (Figure 4). Inherited zircon cores yield a large range in concordant ages. Single inherited cores yield $^{206}Pb/^{238}U$ ages of 2772 ± 59 Ma, 629 ± 11 Ma and 378.7 ± 4.8 Ma, while two small groups of three inherited cores each yield the concordia ages of 541.8 ± 6.7 Ma (MSWD = 0.53), and 417 ± 11 Ma (MSWD = 0.57; Figure 5a; Table 5). Three grains with oscillatory magmatic zonation and six oscillatory zoned rims on the inherited cores yield an age of 315.9 ± 2.6 Ma (MSWD = 0.69; Figure 5b; Table 5). One concordant analysis with large uncertainty was also determined but supported this late Variscan age. Th/U ratios range from 0.10 to 1.14 (Table 5) both in cores and in rims.

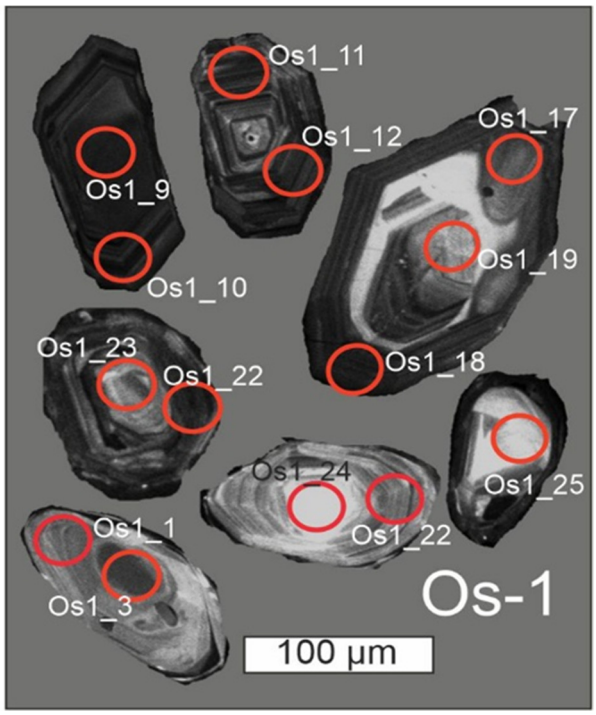

Figure 4. Cathodoluminescence (CL) images of selected zircon crystals from granitoid from Osielec granite. Selected analytical spots and analysis numbers (see Table 6) are marked as circles.

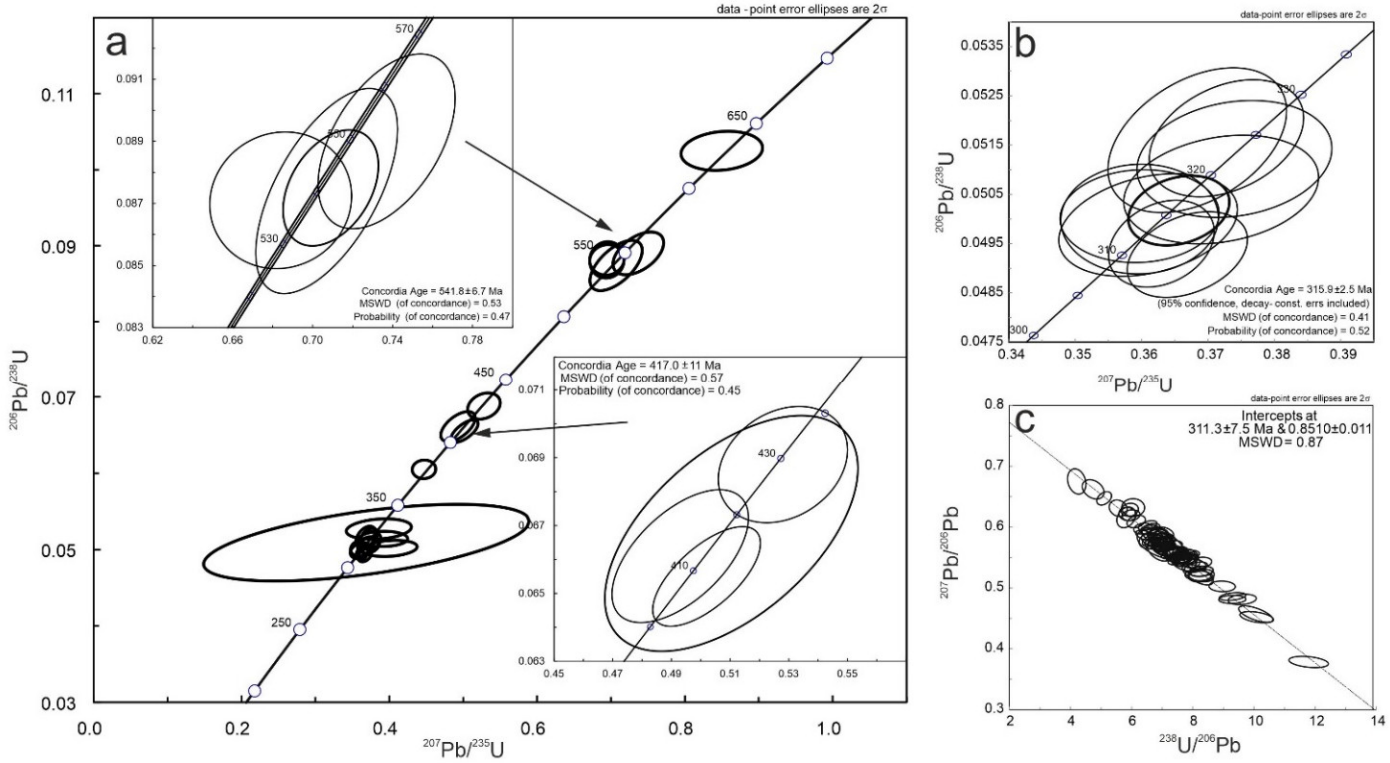

Figure 5. Concordia plots of LA-ICP-MS zircon analytical results from Osielec granite with inserts of inherited cores (**a**), concordia plot of the main magmatic age (**b**) and Tera-Wasserburg concordia plot for apatite from Osielec granite (**c**).

4.2.2. Apatite Morphology and U-Pb Dating

Apatite crystals are clear, translucent and idiomorphic hexagonal prisms, with aspect ratios ranging from 1.5:1 to 4:1 and long axes ranging from 150 to 600 µm. They are zoned in respect to REE, with $\sum_{REE}$ ranging from 3135 ppm (at rims) to 10,758 ppm (in cores) (Table S1). Their chondrite(C1)-normalized REE patterns show LREE enrichment (Ce/Yb = 15.1–43.3) and negative Eu anomalies (Eu/Eu* = 0.52–0.61; Table S1; Figure 3c). Eighty-three analyses from 46 grains yield an unanchored Tera-Wasserburg lower intercept age of 311.3 ± 7.5 with a $^{207}Pb/^{206}Pb$ initial ratio of 0.851 ± 0.011 (MSWD = 0.87; Figure 5c; Table S2).

5. Discussion

5.1. Petrogenetic Interpretation

The granitoid from Osielec belongs to the high-K–calc-alkaline series (Figure 3b) and plots in the Volcanic Arc Granite (VAG) field (Figure 6). On a primitive mantle–normalized multielement diagram (Figure 3d), the characteristic negative Nb and Ta anomalies are very flat and cannot be considered as diagnostic. The high Zr saturation temperatures and anti-rapakivi mantling on K-feldspars (Figure 2), as well as the high Ba and Sr contents, imply at least a component of mantle derivation. Fractionated chondrite-normalized REE patterns, with very weak negative Eu anomalies (Figure 3c), are typical of oxidized mantle-influenced melts. This is supported by the whole-rock isotopic characteristics (recalculated at 316 Ma): a low initial Sr ratio of 0.704710 and positive $\varepsilon Nd_{(316\,Ma)}$ value of 2.15 (Table 6) imply a mantle-related affinity of the parent magma. The high Th/U ratio in the whole-rock samples, in zircon (Table 5) and in apatite (Table S1) suggests a Th-enriched mantle and/or fluid influence during magma formation [36]. The T_{DM} model age of 1.18 Ga (Table 6) is younger than the crustal residence ages typical of the Variscan fold belt of Europe (1.4–1.8 Ga; [37]), as most of the post-tectonic granites in the Variscan belt of Europe reflect the mixture of Cadomian/Caledonian and Paleoproterozoic source involvement [38]. The presence of inherited cores in the zircon crystal population covers a wide age range from c. 2772 Ma to c. 417 Ma and support this interpretation.

Table 6. Sm-Nd and Rb-Sr whole-rock isotopic data from the exotic crystalline block from Oseilec.

Sample	Rb (ppm)	Sr (ppm)	$^{87}Rb/^{86}Sr$	$^{87}Sr/^{86}Sr$	±	ISr_{316}	Sm (ppm)	Nd (ppm)	$^{147}Sm/^{144}Nd$	$^{143}Nd/^{144}Nd$	±	$\varepsilon_{Nd}{}^{316}$	T_{DM}
Osielec	139.8	1116	0.357738	0.706319	0.000003	0.704710	7.22	52	0.083936	0.512312	0.000004	2.15	1.18 Ga

A minimum closure temperature of c. 900 °C is assumed for Pb diffusion in zircon, while the Pb partial retention zone is c. 450–550 °C in apatite [39–41]. Therefore, the zircon and apatite U-Pb ages overlap within age uncertainty suggesting relatively fast cooling, inconsistent with monotonic thermal relaxation of a pluton at depth. Therefore, the mantle-derived magma intrusion either intruded at a shallow crustal level and/or was rapidly exhumed during cooling. Such a scenario is typical of post-collisional mantle lithosphere delamination. This process is common in the late-Variscan evolution of the Central European Orogenic Belt ([42,43] and references therein) and is assumed responsible for the emplacement of voluminous I-type granitoids associated with the rapid exhumation and a low-pressure-high-temperature metamorphic overprint. The high Th/U ratios found in the analyzed zircon crystals (Table 6), both in the magmatically zoned rims and in the cores, are typical of the magmatic process [44] and exclude metamorphic overprinting.

5.2. Source Region of the Exotic Clasts

Exotic blocks are only sporadically found within the Magura Nappe. The available age data include a metadiorite-metagabbro dated at c. 614 Ma [7,9], centimeter-scale mica-schist pebbles from the Tylicz and Krynica Zone dated at 310 ± 10 Ma using the U-Th-Pb CHIME method on monazite [45] and the porphyritic granite dated in this study at 315.9 ± 2.6 Ma. The presence of clasts of both Neoproterozoic ocean floor remnants (gabbro-diorite) and

Late Variscan I-type granites and metapelitic rocks suggests that the Fore-Magura Ridge could contain fragments of the Neoproterozoic basement, locally intruded and thermally metamorphosed by the Variscan granites. The Cadomian age of the inherited zircon cores in the investigated granitoid (541.8 ± 6.7 Ma; Table 5, Figure 5a), together with the presence of blocks of Neoproterozoic age (c. 614 Ma; [7]), suggest that peri-Gondwana basement was incorporated within this Variscan tectono-magmatic belt, as has been documented in many segments of the Variscan orogen (cf. [46–48]). No granites with similar zircon U-Pb ages and petrological characteristics have been noted in the Central Western Carpathians, in the Silesian and Subsilesian Nappes of the Outer Carpathians, or in Brunovistulia and the Małopolska Block. This, together with the lack of detrital fragments from the Pieniny Klippen Belt [45], implies there was no link between the Central Carpathians and Outer Carpathian basins during the Cretaceous to Paleogene. There is also no correlation between the basement of the Magura Nappe and the Silesian and Subsilesian Nappes.

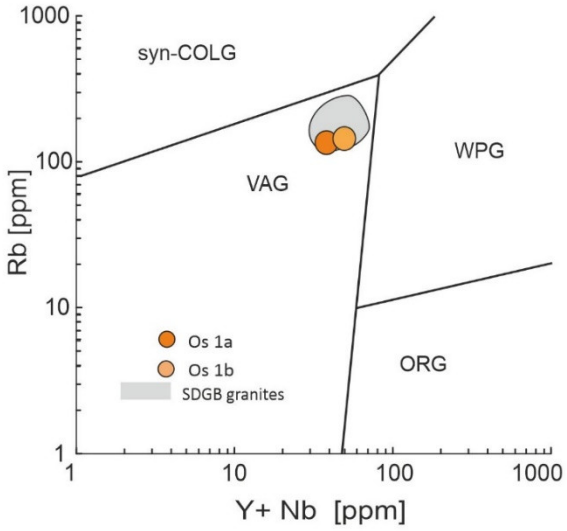

Figure 6. Plot of the granitoid from Osielec stream on the discrimination diagram of [49]: VAG—volcanic arc granites; syn-COLG—syn-collisional granites, WPG—within-plate granites, ORG—ocean ridge granites.

Similar U-Pb ages and geochemical characteristics to the Osielec granitoid samples investigated in this study are exhibited by the Saxoturingian and Moldanubian granites in the Saxo-Danubian Granite Belt (SDGB), such as the Falkenberg and Liebenstein granites (dated at 330–310 Ma, [50,51] and references therein), the Strzelin granites (Oberc-Dziedzic et al. 2016 [52] and references therein) and the Karkonosze granite [53]. The Karkonosze granite is an unlikely source taking into account its paleogeographic position [54]. As the youngest varieties (315–310 Ma) of the SDGB granitoids are fine- to medium-grained S-type migmatitic granites, we propose that a more likely source is the older (320–328 Ma), genetically mixed (S/I) type) coarse-grained granitoids with K-feldspar phenocrysts in the SDGB, with geochemical features indicative of mantle delamination or a slab-break-off origin [35,52]. The first model is more preferred for the South Bohemian Massif, with assumed lithosphere thinning and extension, followed by mantle melting [54]. These processes produced mantle-type melts up to c. 305 Ma and were followed by transtension in the Central European segment of Variscides [55]. The metagabbro-metadiorite exotic blocks [7] could have counterparts in the Cadomian mafic intrusions, which are found at the Moldanubian-Moravian Unit boundary ([51,56] and references therein). The Moldanubian zone, originally described in the southern part of the Bohemian Massif between the Vltava (Moldau) and Danube rivers, probably extended westwards into the Black Forest in Germany, the southern Vosges Massif, the Massif Central, Nort-sur-Erdre; the South Armorican unit in France and into the Galicia-Trás-os-Montes zone in Spain (Figure 7). It also

includes Corsica and the external crystalline massifs of the Alps. The ophiolitic parts of the Moldanubian zone represent a probable oceanic realm, the so-called Galicia-Moldanubian Ocean, which connected the eastern and western parts of the Paleotethys Ocean [57,58].

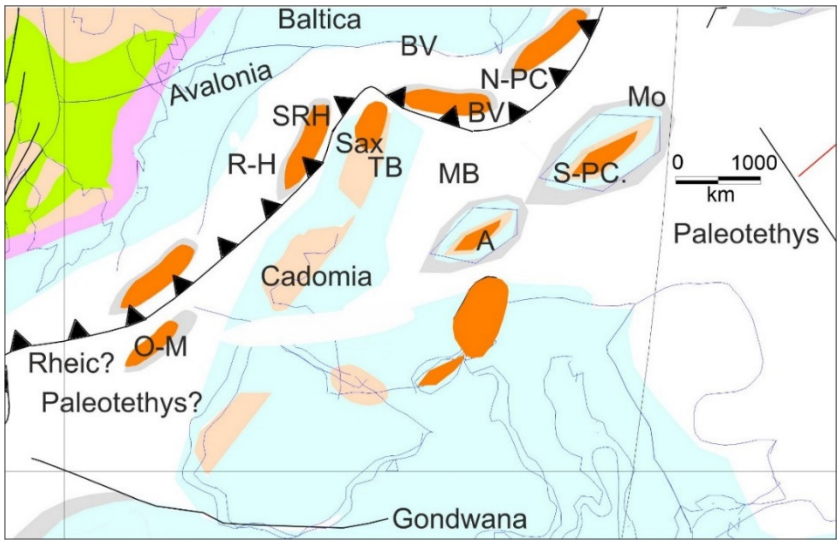

Figure 7. Paleogeography of the peri-Gondwanan domains on the Laurussia and European margins (central–southern Europe) during the Late Devonian (modified from [57]). Abbreviations: A—alpine terranes, BV—Brunovistulicum, MB—Moldanubian (Galicia-Moldanubian Ocean), MGC—Mid-German Crystalline Zone, MGU—Meguma terranes, Mo—Moesia, N-PC—Northern Proto-Carpathian and Balkan terranes, R-H—Rheno-Hercynian, Sax—Saxothuringia, S-PC—Southern Proto-Carpathian and Balkan terranes, SRH—Southern Rheno-Hercynian, TB—Tepla-Barrandian.

The exotic rocks deposited in the Magura Basin constituted part of the Alpine Tethys [14]. Based on models recently applied to the Alps, we can link the formation of this basin to strike-slip transform faulting, which occurs in the Early to Middle Jurassic that resulted in the opening of the South Penninic–Piedmont–Ligurian Ocean ([59,60] and references therein). The Magura Ocean has been suggested to be an eastern prolongation of that ocean.

As a result of Alpine compression, the ridges separating the Carpathian subbasins were uplifted and inverted during the Late Cretaceous to Paleogene. These ridges from north to south comprise the Sub-Silesian, Silesian and Fore-Magura Ridges ([60,61] and references therein) (Figure 8a,b). Intensive erosion of the ridges, driven by tectonic uplift, resulted in the transport of the crystalline basement as clastic material to the basins, locally as olistostromes.

The Fore-Magura Ridge developed within the northern part of the Magura Domain during the Late Cretaceous [14,62]. This ridge was eroded during the Paleogene, exposing the crystalline basement. In the Magura Basin, sediment transport was likely derived from the Fore-Magura Ridge (Figure 8c; [9,63,64]). The distribution of exotic crystalline clasts reflects the zonation of the Variscan orogen in the Outer Carpathians. The southern zone (Foremagura Ridge) represents the internal core of the Variscan collisional orogen, while the northern zone (Silesian Ridge and Outer Carpathian Basement) represents the Variscan foreland built of Neoproterozoic rocks. As the large exotic blocks are assumed to have not been transported for significant distances, we infer that the crystalline basement of the Fore-Magura Ridge is comprised of Moldanubian Unit rocks.

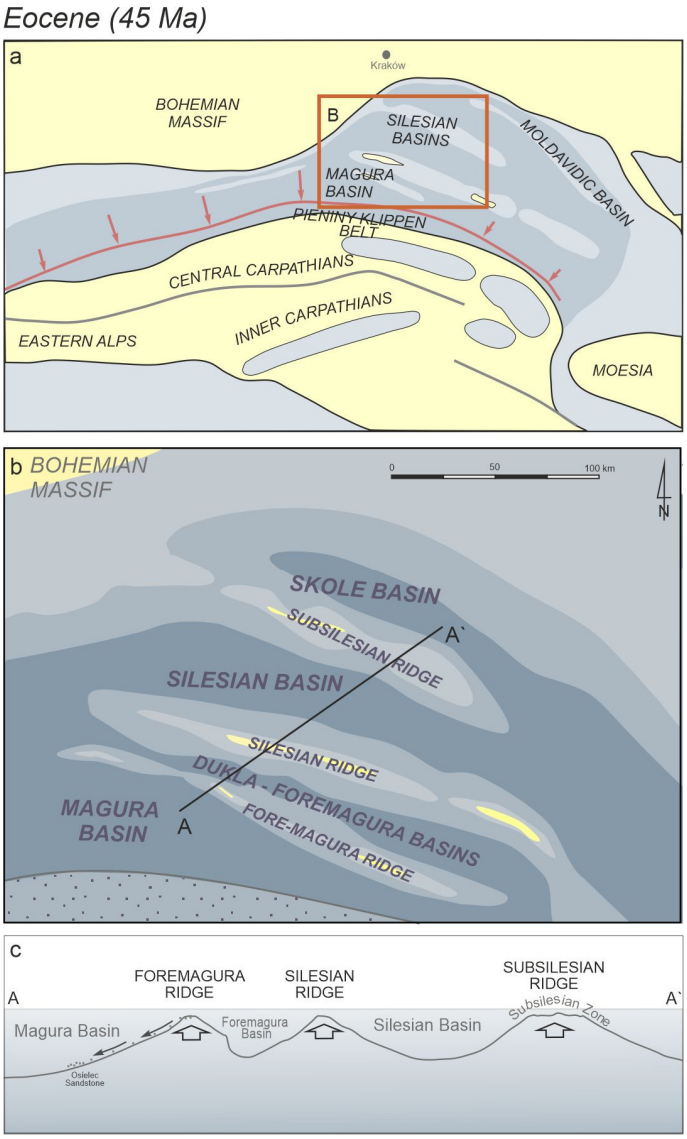

Figure 8. (**a**,**b**) Paleogeographic reconstruction of the circum-Carpathians area (**c**) with a palinspastic cross-section in the Early Paleogene [1].

6. Conclusions

The main conclusions arising from this study are:

(1) The exotic block from Osielec represents an I-type, oxidized mantle-related late Variscan (post-orogenic) granitoid, probably related to magmatic underplating. The timing of crystallization is constrained by a U-Pb zircon date of 315.9 ± 2.6 Ma, while a U-Pb apatite age of 311.3 ± 7.5 Ma, which overlaps within age uncertainty, implies rapid cooling.

(2) As the large exotic blocks are not far traveled, the presence of this late Variscan granite clast in the Fore-Magura Ridge implies an affinity with the Moldanubian Unit (Saxo-Danubian Granite Belt) in the Central European Variscides.

Supplementary Materials: The following are available online at https://www.mdpi.com/2075-163X/11/3/256/s1, Table S1: Representative LA-ICP-MS U–Pb apatite data from the Osielec sample, Poland; Table S2: Trace element (including rare earth elements) concentrations (in ppm) and main petrogenetic indices.

Author Contributions: A.G.: corresponding author, project formulation, fieldwork, zircon selection, U-Pb age calculation and presentation, petrological description and interpretation, final discussion; K.S.: fieldwork, zircon imaging by cathodoluminescence, petrological descriptions, final discussion; J.G.: project formulation, fieldwork and sampling, paleotectonic reconstructions, final discussions; D.C.: zircon U-Pb analyses, discussion of U-Pb zircon age meaning in the context of the paleotectonic reconstruction, final discussions and editing; A.W.: fieldwork, sampling, lithological correlations, geological map preparation, final discussion. All authors have read and agreed to the published version of the manuscript.

Funding: This study was supported by National Science Centre (NCN) grant 2016/23/B/ST10/01896 given to J.G., A.G., A.W. and K.S. D.C. acknowledges past and present support from Science Foundation Ireland through research grants 12/IP/1663, 13/RC/2092 (iCRAG Research Centre), and 15/IA/3024. iCRAG is funded under the SFI Research Centres Programme and is co-funded under the European Regional Development Fund.

Acknowledgments: The authors thank Beata Marciniak-Maliszewska for her help during microprobe analyses, while Monika Horschinegg is acknowledged for the help in the Nd and Sr isotope whole-rock work. The manuscript benefited from the comments of 3 anonymous reviewers. Authors are very grateful for their work.

Conflicts of Interest: The authors declare no conflict of interest. The funders had no role in the design of the study, in the collection, analyses, or interpretation of data, in the writing of the manuscript, or in the decision to publish the results.

References

1. Golonka, J.; Gawęda, A.; Waśkowska, A. Carpathians. In *Encyclopedia of Geology*, 2nd ed.; Alderon, D., Elias, S.A., Eds.; Elsevier: Amsterdam, The Netherlands, 2021; pp. 372–381. [CrossRef]
2. Andersen, T. Detrital zircons as tracers of sedimentary provenance: Limiting conditions from statistics and numerical simulation. *Chem. Geo.* **2005**, *216*, 249–270. [CrossRef]
3. O'Sullivan, G.; Chew, D.; Kenny, G.; Henrichs, I.; Mulligan, D. The trace element composition of apatite and its application to detrital provenance studies. *Earth. Sci. Rev.* **2020**, *201*, 103044. [CrossRef]
4. Burda, J.; Woskowicz-Ślęzak, B.; Klötzli, U.; Gawęda, A. Cadomian protolith ages of exotic mega blocks from Bugaj and Andrychów (Western Outer Carpathians, Poland) and their palaeogeographic significance. *Geochronometria* **2019**, *46*, 25–36. [CrossRef]
5. Budzyń, B.; Dunkley, D.J.; Kusiak, M.A.; Poprawa, P.; Malata, T.; Skiba, M.; Paszkowski, M. SHRIMP U-Pb zircon chronology of the Polish Western Outer Carpatians source areas. *Ann. Soc. Geol. Poloniae* **2011**, *81*, 161–171.
6. Cieszkowski, M.; Golonka, J.; Ślączka, A.; Waśkowska, A. Role of the olistostromes and olistoliths in tectonostratigraphic evolution of the Silesian Basin in the Outer Carpathians. *Tectonophysics* **2012**, *568–569*, 248–265. [CrossRef]
7. Gawęda, A.; Golonka, J.; Waśkowska, A.; Szopa, K.; Chew, D.; Starzec, K.; Wieczorek, A. Neoproterozoic crystalline exotic clasts in the Polish Outer Carpathian flysch: Remnants of the Proto-Carpathian continent? *Int. J. Earth. Sci.* **2019**, *108*, 1409–1427. [CrossRef]
8. Wieser, T. The ophiolithe from Osielec. *Ann. Soc. Geol. Poloniae* **1952**, *21*, 319–327.
9. Cieszkowski, M.; Kysiak, T.; Szczęch, M.; Wolska, A. Geology of the Magura Nappe in the Osielec area with emphasis on an Eocene olistostrome with metabasite olistoliths (Outer Carpathians, Poland). *Ann. Soc. Geol. Poloniae* **2017**, *87*, 169–182. [CrossRef]
10. Golonka, J.; Krobicki, M.; Matyszkiewicz, J.; Olszewska, B.; Ślączka, A.; Słomka, T. Geodynamics of ridges and development of carbonate platform within the Carpathian realm in Poland. *Slovak Geol. Mag.* **2005**, *11*, 5–16.
11. Ślączka, A.; Kruglow, S.; Golonka, J.; Oszczypko, N.; Popadyuk, I. The General Geology of the Outer Carpathians, Poland, Slovakia, and Ukraine. In *The Carpathians and Their Foreland: Geology and Hydrocarbon Resources*, 1st ed.; Golonka, J., Picha, F., Eds.; American Association of Petroleum Geologists: Tulsa, OK, USA, 2006; Volume 84, pp. 221–258.
12. Oszczypko, N.; Oszczypko-Clowes, M. Stages in the Magura Basin: A case study of the Polish sector (Western Carpathians). *Geodin. Acta* **2009**, *22*, 83–100. [CrossRef]
13. Oszczypko, N.; Ślączka, A.; Oszczypko-Clowes, M.; Olszewska, B. Where was the Magura ocean? *Acta Geol. Pol.* **2015**, *65*, 319–344. [CrossRef]
14. Golonka, J.; Waśkowska, A.; Ślączka, A. The Western Outer Carpathians: Origin and evolution. *Z. Geol. Wiss.* **2019**, *170*, 229–254. [CrossRef]
15. Koszarski, L.; Sikora, W.; Wdowiarz, S. The Flysch Carpathians. Polish Carpathians. In *Tectonics of the Carpathian–Balkan Regions. Explanations to the Tectonic Map of the Carpathian-Balkan Regions and their Foreland*; Mahel, M., Ed.; Štátny geologický ústav Dionýza Štúra: Bratislava, Slovakia, 1974; pp. 180–197.

16. Golonka, J.; Ślączka, A.; Waśkowska, A.; Krobicki, M.; Cieszkowski, M. Budowa geologiczna zachodniej części polskich Karpat zewnętrznych. In *Głębokomorska Sedymentacja Fliszowa—Sedymentologiczne Aspekty Historii Basenów Karpackich. V Polska Konferencja Sedymentologiczna*; Krobicki, M., Feldman-Olszewska, A., Eds.; Państwowy Instytut Geologiczny-Państwowy Instytut Badawczy: Warszawa, Poland, 2013; pp. 11–62.
17. Książkiewicz, M. Geologia Regionu Babiogórskiego. In *Przewodnik 39 Zjazdu Polskiego Towarzystwa Geologicznego 2–5 Czerwca*; Wydawnictwa Geologiczne: Warszawa, Poland, 1966; pp. 5–58. (In Polish)
18. McDonough, W.F.; Sun, S.S. The composition of the Earth. *Chem. Geol.* **1995**, *120*, 223–253. [CrossRef]
19. Petrus, J.A.; Kamber, B.S. VizualAge: A Novel Approach to Laser Ablation ICP-MS U-Pb Geochronology Data Reduction. *Geostand. Geoanal. Res.* **2012**, *36*, 247–270. [CrossRef]
20. Paton, C.; Helistrom, J.; Paul, B.; Woodhead, J.; Herqt, J. Iolite: Freeware for the visualisation and processing of mass spectrometric data. *J. Anal. Atom. Spectrom.* **2011**, *26*, 2508–2518. [CrossRef]
21. Ludwig, K.R. *Isoplot/Ex, v. 4.75*; Berkeley Geochronology Center Special Publication: Berkeley, CA, USA, 2012; p. 5.
22. Wiedenbeck, M.A.P.C.; Alle, P.; Corfu, F.; Griffin, W.L.; Meier, M.; Oberli, F.V.; Spiegel, W. Three natural zircon standards for U-Th-Pb, Lu-Hf, trace element and REE analyses. *Geostand. Geoanal. Res.* **2005**, *19*, 1–23. [CrossRef]
23. Nasdala, L.; Corfu, F.; Schoene, B.; Tapster, S.R.; Wall, C.J.; Schmitz, M.D.; Ovtcharova, M.; Schaltegger, U.; Kennedy, A.K.; Kronz, A.; et al. GZ7 and GZ8—Two Zircon Reference Materials for SIMS U-Pb Geochronology. *Geostand. Geoanal. Res.* **2018**, *42*, 431–457. [CrossRef]
24. Sláma, J.; Košler, J.; Condon, D.J.; Crowley, J.L.; Gerdes, A.; Hanchar, J.M.; Schaltegger, U. Plešovice zircon—A new natural reference material for U–Pb and Hf isotopic microanalysis. *Chem. Geol.* **2008**, *249*, 1–35. [CrossRef]
25. Pointon, M.A.; Cliff, R.A.; Chew, D.M. The provenance of Western Irish Namurian Basin sedimentary strata inferred using detrital zircon U–Pb LA-ICP-MS geochronology. *Geol. J.* **2012**, *47*, 77–98. [CrossRef]
26. Chew, D.M.; Donelick, R.A. Combined apatite fission track and U-Pb dating by LAICPMS and future trends in apatite provenance analysis. In *Quantitative Mineralogy and Microanalysis of Sediments and Sedimentary Rocks*; Sylvester, P., Ed.; Mineralogical Association of Canada: Québec, QC, Canada, 2012; pp. 219–248.
27. Schoene, B.; Bowring, S.A. U-Pb systematics of the McClure Mountain syenite: Thermochronological constraints on the age of the Ar-40/Ar-39 standard MMhb. *Contrib. Mineral. Petrol.* **2006**, *151*, 615–630. [CrossRef]
28. Chew, D.; Babechuk, M.G.; Cogne, M.; Mark, C.; O'Sullivan, G.J.; Henrichs, I.A.; Doepke, D.; McKenna, C.A. (LA,Q)-ICPMS trace element analyses of Durango and McClure Mountain apatite and implications for making natural LA-ICPMS mineral standard. *Chem. Geol.* **2016**, *435*, 35–48. [CrossRef]
29. Chew, D.M.; Petrus, J.A.; Kamber, B.S. U-Pb LA-ICPMS dating using accessory mineral standards with variable common Pb. *Chem. Geol.* **2014**, *363*, 185–199. [CrossRef]
30. McDowell, F.; McIntosh, W.C.; Farley, K.A. A precise 40Ar–39Ar reference age for the Durango apatite (U–Th)/He and fission-track dating standard. *Chem. Geol.* **2005**, *214*, 249–263. [CrossRef]
31. Watson, T.M.; Harrison, E.B. Zircon saturation revisited: Temperature and composition effects in a variety of crustal magma types. *Earth. Planet. Sci. Lett.* **1983**, *64*, 295–304. [CrossRef]
32. Ridolfi, F.; Renzulli, A.; Puerini, M. Stability and chemical equilibrium of amphibole in calc-alkaline magmas: An overview, new thermometric formulation and application to subduction-related volcanoes. *Contrib. Mineral. Petrol.* **2010**, *160*, 45–66. [CrossRef]
33. Middlemost, E.A.K. *Magmas and Magmatic Rocks. An Introduction to Igneous Petrology*; Longman Group Ltd.: London, UK, 1985; p. 266.
34. Peccerillo, A.; Taylor, S.R. Geochemistry of Eocene calc-alkaline volcanic rocks from the Kastamonu area, northern Turkey. *Contrib. Mineral. Petrol.* **1976**, *58*, 63–81. [CrossRef]
35. Gerdes, A. Magma homogenization during anatexis, ascent and/or emplacement? Constraints from Variscan Weinsberg Granites. *Terra Nova* **2001**, *13*, 305–312. [CrossRef]
36. Rudnick, R.; Gao, S. Composition of the continental crust. *Treatise Geochem.* **2004**, *3*, 1–64.
37. Liew, T.C.; Hofmann, A.W. Precambrian crustal components, plutonic associations, plate environment of the Hrcynian Fold Belt of Central Europe: Indications from a Nd and Sr isotopic study. *Contrib. Mineral. Petrol.* **1988**, *98*, 129–138. [CrossRef]
38. Moyen, J.F.; Laurent, O.; Chelle-Michou, C.; Couzinié, S.; Vanderhaege, O.; Zeh, A.; Villaros, A.; Gardien, V. Collision vs. subduction-related magmatism: Two contrasting ways of granite formation and implications for crustal growth. *Lithos* **2017**, *277*, 154–177. [CrossRef]
39. Cherniak, D.J. Diffusion in accessory minerals: Zircon, titanite, apatite, monazite and xenotime. Rev. *Mineral. Geochem.* **2010**, *72*, 827–869. [CrossRef]
40. Chamberlain, K.R.; Bowring, S.A. Apatite-feldspar U-Pb thermochronometer: A reliable, mid-range (450 °C), diffusion controlled system. *Chem. Geol.* **2000**, *172*, 173–200. [CrossRef]
41. Schoene, B.; Bowring, S.A. Determining accurate temperature-time paths from U-Pb thermochronology: An example from the Kaapval craton, southern Africa. *Geochim. Cosmochim. Acta* **2007**, *71*, 165–185. [CrossRef]
42. Zulauf, G. Von der Anchizone bis zur Eklogitfazies: Angekippte Krustenprofile als Folge der cadomischen und variscischen Orogenese im Teplá-Barrandium (Böhmische Masse). *Geotekt. Forsch.* **1997**, *89*, 1–302.
43. Medaris, G., Jr.; Wang, H.; Jelínek, E.; Mihaljevič, M.; Jakeš, P. Characteristics and origins of diverse Variscan peridotites in the Gföhl Nappe, Bohemian Massif, Czech Republic. *Lithos* **2005**, *82*, 1–23. [CrossRef]

44. Rubatto, D. Zircon trace element geochemistry: Partitioning with garnet and the link between U–Pb ages and metamorphism. *Chem. Geol.* **2002**, *184*, 123–138. [CrossRef]
45. Oszczypko, N.; Salata, D.; Konečny, P. Age and provenance of mica-schist pebbles from the Eocene conglomerates of the Tylicz and Krynica Zone (Magura Nappe, Outer Caarpathians). *Geol. Carp.* **2016**, *67*, 257–271. [CrossRef]
46. Gawęda, A.; Burda, J.; Klötzli, U.; Golonka, J.; Szopa, K. Episodic construction of the Tatra granitoid intrusion (Central Western Carpathians, Poland/Slovakia): Consequences for the geodynamics of Variscan collision and Rheic Ocean closure. *Int. J. Earth. Sci.* **2016**, *105*, 1153–1174. [CrossRef]
47. Gawęda, A.; Szopa, K.; Włodyka, R.; Burda, J.; Crowley, Q.G.; Sikorska, M. Continuous magma mixing and cumulate separation in the High Tatra Mountains open system granitoid intrusion, Western Carpathians (Poland/Slovakia): A textural and geochemical study. *Acta Geol. Pol.* **2019**, *69*, 549–570. [CrossRef]
48. Awdankiewicz, M.; Awdaniewicz, H.; Kryza, R.; Rodionow, N. SHRIMP zircon study of a micromonzodiorite dyke in the Karkonosze Granite, Sudetes (SW Poland): Age constraints for late Variscan magmatism in Central Europe. *Geo. Mag.* **2000**, *147*, 77–85. [CrossRef]
49. Pearce, J.A.; Harris, N.B.W.; Tindle, A.G. Trace elements discrimination diagram for the tectonic interpretation of granitic rocks. *J. Petrol.* **1984**, *25*, 956–983. [CrossRef]
50. Siebel, W.; Chen, F.; Satir, M. Late-Variscan magmatism revisited: New implications from Pb-evaporation zircon ages on the emplacement of redwitzites and granites in NE Bavaria. *Int. J. Earth. Sci.* **2003**, *92*, 36–53. [CrossRef]
51. Finger, F.; Gerdes, A.; René, M.; Riegler, G. The Saxo-Danubian Granite Belt: Magmatic response to post-collisional delamination of mantle lithosphere below the sout-western sector of the Bohemian Massif (Variscan orogen). *Geol. Carp.* **2009**, *60*, 205–212. [CrossRef]
52. Oberc-Dziedzic, T.; Pin, C.; Madej, S.; Kryza, R. Three generations of granitoids emplaced over a 300 My time span in the Strzelin Massif, Fore-Sudetic Block, SW Poland: Mutual relationships and implications for secular crustal evolution. *J. Geosci.* **2016**, *61*, 289–308. [CrossRef]
53. Kryza, R.; Pin, C.; Oberc-Dziedzic, T.; Crowley, Q.G.; Larionov, A. Deciphering the geochronology of a large granitoid pluton (Karkonosze Granite, SW Poland): An assessment of U–Pb zircon SIMS and Rb–Sr whole-rock dates relative to U–Pb zircon CA-ID-TIMS. *Int. Geol. Rev.* **2014**, *56*, 756–782. [CrossRef]
54. Mazur, S.; Aleksandrowski, P.; Turniak, K.; Awdankiewicz, M. Geology, tectonic evolution and Late Palaeozoic magmatism of Sudetes—An overview. Granitoids in Poland. *AM Monogr.* **2007**, *1*, 59–87.
55. Mazur, S.; Aleksandrowski, P.; Gągała, Ł.; Krzywiec, P.; Żaba, J.; Gaidzik, K.; Sikora, R. Late Palaeozoic strike-slip tectonics versus oroclinal bending at the SW outskirts of Baltica: Case of the Variscan belt's eastern end in Poland. *Int. J. Earth. Sci.* **2020**, *109*, 1133–1160. [CrossRef]
56. Ulrych, J.; Ackerman, L.; Kachlik, V.; Hegner, E.; Balogh, K.; Langrova, A.; Luna, J.; Fediuk, F.; Lang, M.; Filip, J. Constraints on the origin of gabbroic rocks from the Moldanubian-Moravian units boundary (Bohemian Massif, Czech Republic and Austria). *Geol. Carp.* **2010**, *61*, 175–191. [CrossRef]
57. Golonka, J. Late Devonian paleogeography in the framework of global plate tectonics. *Glob. Planet. Chang.* **2020**, *186*, 103129. [CrossRef]
58. Martínez Catalán, J.R.; Collett, S.; Schulmann, K.; Aleksandrowski, P.; Mazur, S. Correlation of allochthonous terranes and major tectonostratigraphic domains between NW Iberia and the Bohemian Massif, European Variscan belt. *Int. J. Earth Sci.* **2020**, *109*, 1105–1131. [CrossRef]
59. Haas, I.; Eichinger, S.; Haller, D.; Fritz, H.; Nievoll, J.; Mandl, M.; Hippler, D.; Hauzenberger, C. Gondwana fragments in the Eastern Alps: A travel story from U/Pb zircon data. *Gondwana Res.* **2020**, *77*, 204–222. [CrossRef]
60. Plašienka, D. Jurassic syn-rift and Cretaceous syn-orogenic, coarse-grained deposits related to opening and closure of the Vahic (South Penninic) Ocean in the Western Carpathians—An overview. *Geol. Q.* **2012**, *56*, 601–628. [CrossRef]
61. Golonka, J.; Waśkowska-Oliwa, A. Stratigraphy of the Polish Flysch Carpathians between Bielsko-Biała and Nowy Targ. Kwartalnik AGH. *Geologia* **2007**, *33*, 5–28.
62. Golonka, J.; Pietsch, K.; Marzec, P. Structure and plate tectonic evolution of the northern Outer Carpathians. In *Tectonics*; Closson, D., Ed.; INTECH: Rijeka, Croatia, 2001; pp. 65–92.
63. Tet'ák, F.; Pivko, D.; Kováčik, M. Depositional systems and paleogeography of Upper Cretaceous-Paleogene deep-sea flysch deposits of the Magura Basin (Western Carpathians). *Palaeogeogr. Palaeoclimatol. Palaeoecol.* **2019**, *533*, 109250. [CrossRef]
64. Bónová, K.; Bóna, J.; Kovačik, M.; Mikuš, T. Heavy minerals and exotic pebbles from the Eocene flysch deposits of the Magura Nappe (Outer Western Carpathians, Eastern Slovakia): Their composition and implications on the provenance. *Turkish J. Earth. Sci.* **2018**, *27*, 64–88. [CrossRef]